Published in final edited form as:
Inorg Chem. 2012 October 15; 51(20): 11098–11105. doi:10.1021/ic301645j.

Revisiting Zinc Coordination in Human Carbonic Anhydrase II

He Song[†], **David L. Wilson**[†], **Erik R. Farquhar**[‡], **Edwin A. Lewis**[†], and **Joseph P. Emerson**[†,*]

[†]Department of Chemistry, Mississippi State University, Mississippi State, MS 39762, USA

[‡]Case Western Reserve University Center for Synchrotron Biosciences, National Synchrotron Light Source, Brookhaven National Laboratory, Upton, NY 11973, USA

Abstract

Carbonic anhydrase (CA) is a well-studied, zinc-dependent metalloenzyme that catalyzes the hydrolysis of carbon dioxide to the bicarbonate ion. The apo-form of CA (apoCA) is relatively easy to generate, and the reconstitution of the human erythrocyte CA has been initially investigated. In the past, these studies have continually relied on equilibrium dialysis measurements to ascertain an extremely strong association constant ($K_a \sim 1.2\times10^{12}$) for Zn^{2+}. However, new reactivity data and isothermal titration calorimetry (ITC) data reported herein call that number into question. As shown in the ITC experiments, the catalytic site binds a stoichiometric quantity of Zn^{2+} with a strong equilibrium constant ($K_a \sim 2 \times 10^9$) that is three orders of magnitude lower than the previously established value. The thermodynamic parameters associated with Zn^{2+} binding to apoCA are unraveled from a series of complex equilibria associated with the *in vitro* metal binding event. This in-depth analysis adds clarity to the complex ion chemistry associated with zinc binding to carbonic anhydrase and validates thermochemical methods that accurately measure association constants and thermodynamic parameters for complex-ion and coordination chemistry observed *in vitro*. Additionally, the zinc sites in both the as-isolated and reconstituted ZnCA were probed using X-ray absorption spectroscopy. Both X-ray absorption near edge structure (XANES) and extended X-ray absorption fine structure (EXAFS) analyses indicate the zinc center in the reconstituted carbonic anhydrase is nearly identical to that of the as-isolated protein and confirms the notion that the metal binding data reported herein is the reconstitution of the zinc active site of human CA II.

Keywords

Carbonic anhydrase; Isothermal Titration Calorimetry; X-ray absorption spectroscopy; Dipicolinic acid; Zinc binding

Introduction

Carbonic anhydrases (CAs) are a family of metalloenzymes that catalyze the zinc-dependent hydrolysis of carbon dioxide (CO_2) to the bicarbonate ion (HCO_3^-).[1-5] Based on primary sequence similarities there are three distinctive classes of CAs (α, β, and γ).[1] Each class of

[*]Corresponding Author Department of Chemistry/Box 9573 Mississippi State University Mississippi State, MS 39762-9573 jemerson@chemistry.msstate.edu telephone: 1(662)325-9500 fax: 1(662)325-1618 .

CA utilizes a catalytic zinc ion bound by either three histidine residues in the α- and γ-classes, or a histidine and two cysteine residues in the β-class of CA.[6] The mechanism of all CAs is generally described as a ping-pong type process,[7] where catalytic turn-over starts with the nucleophilic attack of the carbon atom of CO_2 by a Zn-bound hydroxide ion to generate a zinc-bound bicarbonate complex, which then dissociates from the metal site allowing an additional water to coordinate (equation 1). The bound water is deprotonated rapidly, with the aid of a localized base, to regenerate the catalytic zinc-hydroxide species (equation 2). The nature of the proton shuttle associated with equation 2 appears to be unique to each class of CA.[8]

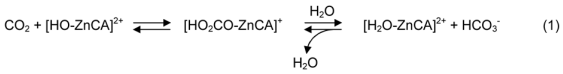

(1)

$$[\mathrm{H_2O} - ZnCA]^{2+} \rightleftarrows [HO - ZnCA]^{+} + \mathrm{H}^{+} \quad (2)$$

The active site of the α-class human CA II has been well studied and details associated with its mechanism have been derived from numerous enzymatic and structural studies.[1] In this system, the tetrahedral zinc center is coordinated with three protein-derived histidine residues (His94, His96, and His119) and a labile water molecule as shown in Figure 1. The zinc ion has been shown to be readily removed from the protein using excess dipicolinic acid (DPA) to create a pseudo-stable metal-free form of both the bovine and human CA II.[1,9,10] This apo-form of human CA II (apoCA) has little to no hydrolytic activity, but can be readily remetallated with a number of transition metals, including Zn^{2+}, where this reconstituted CA (rCA) has similar reactivity with CO_2 as the as-isolated protein. The association constant for zinc binding has been estimated using equilibrium dialysis techniques by Fierke and co-workers to be on the order of 1.2×10^{12},[10,11] and the heat of metal binding has been previously measured.[12] However over the last decade, there have been major advances in our understanding of the complex equilibria associated with zinc binding.[30,40] This new insight has allowed us to generate better thermodynamic models that accurately fit the complex data associated with zinc binding to carbonic anhydrase. Herein, we report new reactivity studies and thermochemical data that suggest the equilibrium constant for zinc binding to CA is about three orders of magnitude lower than previously reported. These thermodynamic parameters associated with zinc binding are calculated based upon a detailed and thorough thermochemical analysis of the zinc binding chemistry of carbonic anhydrase. Additionally, the zinc-binding site of the reconstituted CA was structurally interrogated using X-ray absorption techniques to insure the reconstituted zinc binding site was similar to the metal binding site in the as-isolated protein.

Experimental Section

Reagents and buffers were of the highest grade commercially available and were used as received. All solutions and media were prepared using 18 MΩ water purified by a Millipore ultrapurification system (Millipore, MA, USA).

The plasmid encoding human carbonic anhydrase II (pACA) was kindly provided to our group by C. Fierke. This vector was transformed into *E. coli* BL21(DE3) cells (Agilent Technologies, Santa Clara, CA, USA). All *E. coli* cultures containing this plasmid were grown with shaking at 37 °C in LB media containing 100 mg/L ampicillin. When OD_{600} ~ 0.6, these cultures were induced with 100 mg/L IPTG and allowed to grow for another 4 hours. The *E. coli* cells containing carbonic anhydrase (CA) were frozen and stored at −80 °C. Carbonic anhydrase containing cells were thawed and then lysed in 50 mM Tris buffer (pH 7.0) and the cell extract was concentrated in an Amicon stirred cell with a YM10 membrane. Cell extract was loaded onto a weak DEAE-Sephacel ion-exchange column (GE Healthcare), and fractions were separated using a 500 mM sodium chloride linear gradient. Fractions showing good activity (c.f. esterase activity measurements) were concentrated again as described above and loaded on to a UNOsphereQ Strong anion exchange column (BIO-RAD). Once again, a 500 mM sodium chloride linear gradient was used to separate different biological molecules. Active fractions were concentrated and loaded on to a Sephacryl S-200 size exclusion column (GE Healthcare), which was subjected to an isocratic flow of 50 mM Tris (pH 7.0) buffer with 200 mM sodium chloride. Active fractions that displayed a single band by SDS-PAGE were judged to be pure carbonic anhydrase. The concentration of CA was determined by UV absorption at 280 nm (ε_{280} = 54,000 $M^{-1}cm^{-1}$).[13,14] The preparation of apoCA was performed as follows: CA was first dialyzed overnight against 1 L of 20 mM ACES buffer containing 50 mM dipicolinic acid (pH 7.0) as described previously to generate apoCA.[15,16] Excess dipicolinic acid was removed by dialyzing apoCA versus 2 L of 20 mM Tris (pH 7.0) buffer, then by chromatography using a Sephacryl S-200 size exclusion column. The concentration of apoCA was determined by UV absorption at 280 nm (ε_{280} = 54,000 $M^{-1}cm^{-1}$).[13,14]

Para-nitrophenyl acetate (pNPA) hydrolysis assays were performed as previously described with some modification.[9] All assays were performed in 50 mM BES buffer at pH 7.0. Twenty μL of a 20 mM pNPA/acetonitrile was added to 1 mL of buffer in a disposable cuvette. Up to 20 μL of a protein solution was then mixed into the cuvette and absorption at 404 nm was monitored for 60 seconds. Activity was calculated based on the conversion of pNPA to p-nitrophenol (ε_{404} = 17,300 $M^{-1}cm^{-1}$) and acetate and normalized based assay volumes.

Isothermal titration calorimetry experiments were carried out at 25 °C, unless indicated otherwise, on a MicroCal VP-ITC calorimeter. Samples were buffered at pH 7.4 with 100 mM ACES. A typical experiment consisted of 60 μM apoCA titrated with 1.73 mM $Zn(NO_3)_2$. All solutions were generated with exactly matched buffers and degassed under vacuum prior to running the experiments. The protein concentrations were calculated from known molar absorptivities of both apoCA and native CA.

The ITC data were fitted with the Origin software package provided by MicroCal, and an ITC calorimetry software packaged developed at Mississippi State University, which uses nonlinear least-squares algorithms (minimization of χ^2) and the concentrations of the titrant and the sample to fit the heat flow per injection to equations corresponding to an equilibrium binding model.[17] These fitting programs provide good data simulation and the best-fit values for the stoichiometry (n_{ITC}), change in enthalpy (ΔH_{ITC}), and association constant

(K_{ITC}). Comparison of the goodness of fit with different models was based on the calculated χ^2 value. Three or more good data sets were collected for each type of titration, and the best-fit values were averaged and reported. All ITC data that are presented herein are shown as the baseline-adjusted raw data and the peak integrated, concentration-normalized heat of reaction versus the molar ratio of metal ion to protein. The free energy change for the overall equilibrium of each ITC titration, ΔG_{ITC}, was determined from the equilibrium constant obtained for the best fit of the experimental data, K_{ITC}, as shown in equation 3.

$$\Delta G_{ITC} = -RT\, ln\, K_{ITC} \quad (3)$$

X-ray absorption spectroscopy data was collected at beamline X3B of the National Synchrotron Light Source (NSLS) at Brookhaven National Laboratory. A sagitally focusing Si(111) double crystal monochromator was used for energy selection, with a nickel-coated mirror downstream of the monochromator providing harmonic rejection. Zn-K edge XAS spectra were collected in fluorescence mode over an energy range of 9479 – 10358 eV, using a 31 element Canberra Ge detector. Samples were maintained at a temperature of 20 K under vacuum using a helium Displex cryostat. For internal energy calibration, a zinc foil spectrum was collected concomitantly and its first inflection point was set to 9659 eV.

Two samples (as-isolated carbonic anhydrase: 2.5 mM in 10 mM ACES with 30% glycerol, and reconstituted carbonic anhydrase: 3.0 mM in 10 mM ACES with 30% glycerol) were transferred to Lucite cuvettes covered with Kapton tape as an X-ray transparent window material and quickly frozen in liquid nitrogen. 9 scans were collected and averaged for the as-isolated sample, and 6 scans for the reconstituted sample. Examination of individual scans, averaging, and extraction of the $\chi(k)$ EXAFS was carried out using EXAFSPAK.[18] Specifically, a Gaussian function was fitted to the curved pre-edge background (9479-9635 eV) and this function was subtracted from the entire spectrum to remove background absorption. A 3-segment spline function having 4th order components was fit to the background subtracted data (9630-10363 eV) to extract $\chi(k)$. EXAFS analysis was carried out using the opt program of EXAFSPAK. Theoretical scattering paths were built from the coordinates of a model of the active site of human CA extracted from the crystal structure coordinates (2CBA.pdb), with *ab initio* phase and amplitude parameters for these paths calculated using FEFF 6.[19] Coordination numbers (n) were varied in integer steps while the pathlengths (r) and Debye-Waller factors (σ^2) were allowed to freely float. Coordinated His ligands were simulated using a rigid body approximation,[20] in which the pathlengths of single- and multiple-scattering paths were constrained to a constant difference from one another. The scale factor was fixed at 0.9 in all fits. E_0, the point at which $k = 0$ Å^{-1}, was defined as 9670 eV, and the edge shift parameter ΔE_0 was allowed to float as a single common value for all shells. Fits to Fourier-filtered first-shell EXAFS data used the goodness-of-fit parameter F', defined as $F' = [\sum (\chi_{exptl}-\chi_{calc})^2]^2 / (N_{IDP} - N_{VAR})$, where N_{VAR} is the number of floated variables in the fit, while N_{IDP} is the number of independent data points and is defined as $N_{IDP} = 2\Delta k \Delta r / \pi$. In the latter equation, Δk is the k-range over which the data is fit, while Δr is the back-transformation range employed in fitting Fourier-filtered data. F' provides a useful assessment of the effect of additional shells on improving fit quality.[21] The bond-valence sum (BVS) was also used to assess appropriateness of a

given first-shell fit. The BVS was calculated using $\sum(\exp[(r_0 - r)/0.37])$, where r_0 is an empirically derived parameter for a given pair of atoms (r_0 = 1.776 for Zn^{2+}–N and 1.704 for Zn^{2+}–O) and r is the actual bond length.[22,23] For fits to unfiltered EXAFS data, the goodness of fit F factor was defined as $[\sum k^6(\chi_{exptl}-\chi_{calc})^2 / \sum k^6\chi_{exptl}^2]^{1/2}$.

Results and Discussion

Catalytic hydrolysis of CO_2 is challenging to monitor effectively *in vitro*, so as an alternative activity assay for carbonic anhydrase reactivity, the hydrolysis of p-nitrophenyl acetate (pNPA) to pnitrophenol (pNP) and acetic acid, can be used to measure relative reactivity of carbonic anhydrases (CA) with visible spectroscopy.[9,15,16] The change in absorption at 404 nm can be related to the production of p-nitrophenol (pNP) from this reaction.[9] The as-isolated CA hydrolyzes *p*-NPA to *p*-NP at a rate of 17.9 ± 0.1 mol substrate/min/mol enzyme over background hydrolysis in 50 mM BES at pH 7.0. The apoCA has less than 4% of the reactivity of the as-isolated CA, which is consistent with only a small portion of the apoCA retaining a hydrolytically active metal. By adding a stoichiometric equivalent of Zn^{2+} to apoCA, we are able to fully reconstitute an active form of CA. This reconstituted CA (rCA) hydrolyzes pNPA at a rate of 17.8 ± 0.6 mol substrate/min/mol enzyme, which suggests the enzymatic reactivity is equal within reported error boundaries. This data strongly supports the notion that the Zn^{2+} ion can be both effectively removed and re-incorporated into the active site of CA.

As expected, when rCA is re-exposed to the zinc chelator dipicolinic acid (DPA), the zinc-dependent hydrolytic activity is lost. The fraction of catalytically active enzyme ($ZnCA/CA_o$) in the presence of different equivalents of DPA was established as shown in Figure 2. Approximately 40 equivalents of DPA are required to reduce CA hydrolytic activity by 50%, and nearly all reactivity is lost from rCA when 200 equivalents of DPA are incubated with the protein (Note: Zn-DPA complexes have no measurable hydrolytic activity in the p-NPA assay). Both Kidani and co-workers and Pocker and co-workers have reported similar analyses of inactivation of bovine CA using DPA.[24-26] Association constants for Zn^{2+} can be estimated based on a two competing equilibrium model for DPA-zinc chelation/CA inactivation of carbonic anhydrase as shown in equations 4 and 5. Note the formation constants for Zn^{2+} binding to DPA, log K_{1DPA} = 6.35 and log K_{2DPA} = 5.53.[27]

$$ZnCA + DPA \overset{K_d}{\rightleftarrows} ZnDPA + apoCA \quad (4)$$

$$ZnDPA + DPA \overset{K_{2DPA}}{\rightleftarrows} Zn(DPA)_2 \quad (5)$$

Combining 4 and 5 produces a more generalized expression describing the metal chelation equilibria (equation 6), which in turn yields a mathematical relationship connecting K_{eq} with the K_d term and the concentrations of ZnCA, apoCA, Zn-$(DPA)_2$ and DPA at equilibrium (equation 7).

$$ZnCA+2DPA \overset{K_{eq}}{\rightleftarrows} apoCA+Zn(DPA)_2 \quad (6)$$

$$K_{eq}=K_{\mathrm{d}} \cdot K_2=\frac{[apoCA]_{eq} \cdot [Zn(DPA)_2]_{eq}}{[ZnCA]_{eq} \cdot [DPA]_{eq}^2} \quad (7)$$

If we define the fraction of active enzyme at equilibrium as a function of the initial enzyme concentration of the holoenyzme ZnCA divided by the total enzyme concentration as shown in equation 8.

$$\frac{[ZnCA]_{eq}}{[CA]_0}=\frac{[ZnCA]_{eq}}{\left([apoCA]_{eq}+[ZnCA]_{eq}\right)} \quad (8)$$

And consider the $[DPA]_0 >> [CA]_0$ and assume free $[Zn^{2+}]$ is considered negligible, then it is fair to estimate $[Zn\text{-}(DPA)_2]_{eq} = [apoCA]_{eq}$ and that $[DPA]_{eq} = [DPA]_0$ which allows a mathematical expression for K_{eq} that can be generated with only $[CA]_0$ and $[DPA]_0$ terms (equation 9)[25].

$$K_{eq}=\frac{\left(1-\frac{[ZnCA]_{eq}}{[CA]_0}\right)^2 \cdot [CA]_0^2}{[CA]_0 \cdot \frac{[ZnCA]_{eq}}{[CA]_0} \cdot [DPA]_0^2} \quad (9)$$

The data associated with DPA inactivation was plotted as the fraction of active enzyme versus equivalent of DPA in Figure 2. A curve can be fit to the data in this figure using equation 9, which allows us to calculate a $K_{eq} = 280$ for this process. Combining equations 7 and 9, we can the estimate the association constant (K_a) of Zn^{2+} for apoCA is 2.7×10^9. This estimated value for K_a is three orders of magnitude lower than the values generated from equilibrium dialysis methods.[10,11] However, this simple model associated with metal chelation may neglect a number of related equilibria that could lead to erroneous estimation of the equilibrium constant associated with Zn^{2+} binding to apoCA.

Therefore we also collected data on the metal binding equilibrium associated with coordinating Zn^{2+} to apoCA using isothermal titration calorimetry (ITC). In a single ITC experiment the association constant (K_{ITC}), enthalpy change (ΔH_{ITC}), and binding stoichiometry (n_{ITC}) can all be determined. Specifically the shape of the isotherm gives rise to the equilibrium constant associated with the complex metal binding equilibria between the complex ion species formed between the zinc cation and buffer with the apo-protein's metal binding site.[28] A representative isotherm associated with Zn^{2+} binding to apoCA in ACES buffer and the associated integrated data and a one-site binding model fit are shown in Figure 3.

Although the goal of this project is to measure the thermodynamic values of Zn^{2+} binding to apoCA, the equilibria measured in the ITC are better described as a series of competitive

Zn^{2+} binding equilibria. The data collected in ACES can be simply fit using a one-site binding model (Figure 3), however, serious metal dilution issues are observed in other buffers, which require a more sophisticated analysis. Initially we described these curves as multiple binding events.[29] However, these isotherms can better described as single-site binding events with a number of complicating dilution equilibria. An illustrative case is the data collected in 100 mM PIPES at pH 7.4, shown in Figure 4. Initially this unique curve shape was assigned to two Zn^{2+} binding sites associated with CA, where the second binding site was described as an adventitious metal binding site. The curvature of this endothermic portion of the raw data was actually the result of metal-dilution heat, although the origin of this endothermic dilution process is still unclear. The shape of the integrated raw isotherm (Figure 4, blue trace) past the equivalence point can be corrected by using heats associated with the background titration of $Zn(NO_3)_2$ into PIPES buffer under the same condition (Figure 4, red trace). The heat of dilution in the presence of rCA appears to be more endothermic than in the control reactions. Subtraction of the Zn^{2+}-buffer titration data from the overall integrated raw data affords baseline corrected data (Figure 4, black trace) consistent with a one-site binding event. This analysis is further supported by a complimentary experiment where the reverse titration was performed. ApoCA was titrated into $Zn(NO_3)_2$ under same conditions as described above (Figure S1 in Supporting Information). Initially, the Zn^{2+} concentration in the ITC cell is high, and we observe a large endothermic dilution heat when aliquots of protein are delivered. However, once the metal concentration nears the equivalence point the endothermic process become negligible, which also allows us to measure a similar stability constant (K_{ITC}) and enthalpy of binding (ΔH_{ITC}) for the forward titration in PIPES buffer, thus proving the validity of our analysis. Indeed, we were unable to identify the chemical event generating the endothermic background heats as corresponding to the data collected in PIPES or in ACES buffers. However, we attribute this heat to adventitious metal interactions with both buffer and protein. We applied a similar analysis methodology to the data collected in MOPS and Tris buffers (Figures S2 and S3 in Supporting Information). The ITC data collected in MOPS buffer are very similar to the PIPES data, although a smaller metal dilution heat is observed after the metal binding site is fully occupied. Conversely, the metal dilution heat is very exothermic in Tris buffer, while the shape of curve is clearly that of a single-site binding model. Similar dilution effects were also observed in metal binding studies described by Wilcox and coworkers.[30] The average thermodynamic parameters (K_{ITC} and ΔH_{ITC}) associated with parallel ITC experiments done in at least triplicate for this complex equilibrium were collected in a series of buffers and reported in Table 1. Additionally, the change in free energy, ΔG_{ITC}, and change in entropy, ΔS_{ITC}, associated with the complex equilibria of metal binding were calculated using the following equations: $\Delta G_{ITC} = -RT \ln K_{ITC}$ and $\Delta G_{ITC} = \Delta H_{ITC} - T\Delta S_{ITC}$ (Table 1).

From the Zn^{2+} binding data in a range of buffers, we can unambiguously state that upon binding metal apoCA loses proton density. This notion is evident from the linear dependence of the addition of observed enthalpy from ITC and metal-buffer interaction enthalpy ($\Delta H_{ITC} + \Delta H_{Zn\text{-}Buffer}$) versus the change in enthalpy of ionization for each buffer ($\Delta H_{H\text{-}Buffer}$) as shown in Figure 5. This linear relationship can be fit by equation 10, where

$\Delta H_{H\text{-}Buffer}$, $\Delta H_{Zn\text{-}Buffer}$, $\Delta H_{H\text{-}CA}$ and ΔH_{ZnCA} are heats associated with proton and metal binding to the buffer and apoCA, and n_P is the number of protons released.[32]

$$\Delta H_{ITC} + \Delta H_{Zn-Buffer} = n_p \left(\Delta H_{H-Buffer}\right) + \left(\Delta H_{ZnCA} - n_p \Delta H_{H-CA}\right) \quad (10)$$

By performing our reactions in 100 mM buffer and at pH 7.4, the thermodynamic parameters and speciation of zinc ions in solution are known and favor a well-studied buffer-zinc complex formation.[30] In addition, the high concentration of buffer allows for only a slight reduction in the buffering capacity from buffer-zinc complex formation, while still maintaining a set pH. As a result, the slope of this curve suggests ~ 0.9 protons are displaced by Zn^{2+} binding at pH 7.4, and the y-intercept of this plot, −3.9 kcal/mol, is the enthalpy of Zn^{2+} coordination (ΔH_{ZnCA}) to apoCA minus the protonation enthalpy ($\Delta H_{H\text{-}CA}$) of 0.9 protons of CA.

Furthermore, the buffer- and pH- independent thermodynamic values of zinc binding to apoCA could be derived from a thermodynamic cycle similar to those developed by Wilcox and co-workers.[30,32] The equilibria measured in the ITC are a summation of the dissociation of the buffer-Zn^{2+} complex and the association of Zn^{2+} to the apoCA. We have developed a model for this complex equilibrium involving four simpler equilibria (Table 2). (a) The equilibrium associated with Zn^{2+} release from a complex ion species formed with PIPES buffer, which has been previously investigated and thermodynamic terms reported.[30] (b) Zinc binding to apoCA will result in decreasing the pK_a of the zinc-bound water to 6.8 in the ZnCA complex, and releasing protons to generate a zinc-hydroxide active site.[1,12] (c) The protons released from CA will interact with buffer, and the thermodynamic terms of various buffers are well known.[30,31] (d) Finally, using the data collected from the complex equilibrium and the three previously described simpler equilibria, we can estimate the thermodynamic parameters associated with Zn^{2+} binding to apoCA, which we calculate to be $\Delta H_{ZnCA} = -16.4 \pm 0.1$ kcal/mol and $\Delta G_{ZnCA} = -12.9 \pm 0.1$ kcal/mol in PIPES buffer. The heat of deprotonation of histidine is notably missing from this model. This is due to the fact that the pK_a values associated with the zinc bound histidines, His94, His96, and His119, have been shown to be less than 6 in apoCA,[12,33] suggesting that little to no deprotonation of these resiudes will occur during Zn^{2+} binding to apoCA. The pK_a of the zinc bound water in CA is determined to be 6.8, which suggest as the metal site is formed in CA, approximately 0.8 protons would be released at pH 7.4. This notion is in excellent agreement with our experimentally determined value of 0.9 protons. Similar thermodynamic models can be applied to the other buffer systems studied, which are detailed in the Supporting Information (Table S2 and S3). Since the experimental pH is significantly lower than the pK_a of Tris, we estimate only 24% of Tris is in a deprotonated form. This makes the speciation of the buffer-ion equilibrium too complex to interpret with our current data set, and therefore does not allow us to derive a reasonable stability constant in Tris.

Thermodynamic parameters calculated from titrations of Zn^{2+} into apoCA in various buffers are fully consistent with one another (Table 3). The average pH- and buffer- independent association constant (K_a) of Zn^{2+} for apoCA is 2.2×10^9, which is consistent with the value estimated from the reactivity study presented earlier. This equilibrium constant (or K_d ~ 0.5

nM) suggests CA has a relatively high affinity for Zn^{2+}, which is consistent with our expectations for the native metal ion binding affinity associated with an essential metalloenzyme. The average change in enthalpy of binding is calculated to be −16.2 kcal/mol and the change in entropy is estimated to be −10.2 cal/mol/K (where $-T\Delta S$ = 3.5 kcal/mol). According to our analysis, Zn^{2+} binding to carbonic anhydrase is primarily an enthalpy driven process. The enthalpy value reported here is consistent with the formation of three Zn^{2+}-His bonds, where the $\Delta H°$ for zinc binding to a histidine imidazole is approximately −5 kcal/mol.[40] The unfavorable entropy term measured for Zn^{2+} binding to apoCA is slightly more difficult to interpret. The overall structure of the metal binding site (including mechanistically important water molecules) is nearly identical between the apo- and holo-forms of CA.[41] However there are some structural changes that occur upon Zn^{2+} binding to apoCA, including the ordering of the hydrophilic region of the active site containing the proton shuttle, His64, as well as stabilization of the side-chain residues of several α-helical regions on the outer surface of the enzyme. These structural events could partially account for the unfavorable entropy term associated with our metal binding data. In general, the thermodynamic parameters reported here are significantly different from those reported by DiTusa *et al*.[12] However, it should be noted that the ITC data reported in this 2001 paper seems to be highly consistent with our data. Unfortunately at that time, a more in-depth analysis of the complex equilibria associated with Zn^{2+} binding were not plausible due to the fact that many of the supporting metal-buffer equilibria were uncharacterized.

The reactivity and calorimetry data reported above strongly support the notion that we have reconstituted the Zn-dependent active site of CA. However, to demonstrate that we have rebuilt the Zn-center correctly in rCA, we obtained X-ray absorption spectroscopy data on both the as-isolated and reconstituted CAs. The XANES spectra of as-isolated and reconstituted ZnCA, shown in Figure 6a, are nearly super-imposable, indicating that both enzyme preparations have nearly identical Zn^{2+} sites. The shape and intensity of the edges are consistent with a 4 – 5 coordinate N/O-rich Zn^{2+} site,[34,35] and are quite similar to the XANES spectra previously reported for other ZnCAs containing a $(N_{His})_3O$-Zn^{2+} active site.[7,36,37] Further evidence for very similar Zn^{2+} sites in both the as-isolated and reconstituted forms of CA comes from the near identity of the $k^3\chi(k)$ EXAFS data and the Fourier transforms for both samples (Figure 6b,c). We have carried out a quantitative fitting analysis of the EXAFS for both as-isolated and reconstituted ZnCA, using the coordinates of the Zn^{2+} site in the crystal structure of CA (2CBA.pdb) as a starting point. In both cases, the first coordination sphere can be satisfactorily fit to 4 – 5 N/O ligands at an average distance of 1.98 Å (Table S4, Electronic Supplementary Information). We favor fits with 4 N/O ligands on the basis of bond valence sum calculations. Splitting this single shell into two subshells with 3-4 Zn–N/O scatterers at approximately 2.01 Å and 1-2 Zn–O/N scatterers at ca. 1.90 Å afforded moderate improvements in fit quality. However, the difference in bond lengths was slightly smaller than allowed by the 0.14 Å resolution of the data, and the σ^2 disorder parameters factors for both shells were often implausibly small or even negative, indicating that two-shell fits cannot be justified with the available EXAFS data. The EXAFS data for both samples also shows evidence for the presence of rigid imidazoles, based on the double humped feature present at $k \sim 3\text{-}4$ Å^{-1} in the k^3-weighted EXAFS as well as the shape of the outer-shell features in the FT from r' = 2.4 – 4.0 Å (Figure 6d,e). Multiple-

scattering analysis of these features shows that they are best fit by contributions from 3 symmetrically-bound His ligands (Table 4 and Tables S5 and S6, Electronic Supplementary Information), thus providing a basis for assigning first coordination sphere ligands. We conclude that the Zn^{2+} binding site in both reconstituted and as-isolated human ZnCA consists of 3 nitrogen ligands from histidine and most likely a solvent-derived oxygen atom bound to the Zn^{2+} ion as water/hydroxide.

Our EXAFS fitting results are in good agreement with structural parameters for human ZnCA obtained via X-ray crystallography. We note that the average bond length obtained via EXAFS is some 0.1 Å less than those reported in the crystal structure. This difference can be attributed to several possible factors, including the intrinsic 0.1 – 0.2 Å error for metal-ligand bound lengths determined by macromolecular crystallography (EXAFS-derived bond lengths are typically accurate to ±0.02 Å),[21] packing effects in the crystallized protein that subtly alter coordination geometry, or perhaps temperature effects stemming from the X-ray crystallography and XAS data being collected at radically different temperature (no temperature was reported for the X-ray crystallography measurements).[38] Overall, our XAS data suggests that the zinc metal coordination site of reconstituted CA is for all intents and purposes identical to the zinc active site of the as-isolated CA. This structural data also strongly supports the notion that the heats measured as the zinc center was regenerated are directly related to the zinc ion binding to apoCA.

Conclusions

Whitesides and co-workers have described carbonic anhydrase as an excellent model protein for biophysics, bioanalysis, the physical-organic chemistry of inhibitor design, and medicinal chemistry.[1] This designation requires that every effort should be made to fully understand the thermodynamics of metal binding in CA. Herein we have endeavored to better understand the thermodynamic parameters associated with zinc ion binding to CA. The heats of reaction associated with the complex equilibria measured via isothermical titration calorimetry were analyzed using a method initially proposed by Wilcox and co-workers, [30,32] which allowed us to accurately determine the thermodynamic parameters associated with zinc ion binding to CA. We have shown that the K_a for Zn^{2+} binding apoCA is on the order of 2×10^9 and this process is strongly enthalpy driven. This notion has significant impact on our understanding of the Zn^{2+} binding chemistry of CA. Yet more importantly this work demonstrates the value of this method to the bioinorganic community, which can be used to accurately measure equilibrium constants and thermodynamic parameters associated with complex metal ion coordination chemistry in biological systems.

Supplementary Material

Refer to Web version on PubMed Central for supplementary material.

Acknowledgments

We thank Mississippi State University for start-up funds to J.P.E. to support this research. J.P.E., D.L.W., and H.S. would also like to thank the National Synchrotron Light Source (NSLS) Faculty-Student Research Support Program for funding, which supported our initial XAS training and data collection. All XAS experiments were carried out at beamline X3B of the NSLS at Brookhaven National Laboratory. Beamline X3B is operated by the Case Center for

Synchrotron Biosciences, supported by National Institutes of Health NIBIB Grant P30-EB-009998. NSLS is supported by the United States Department of Energy, Office of Science, Office of Basic Energy Sciences, under Contract DE-AC02-98CH10886. We also thank the National Science Foundation under Grant No. DGE-0947419 at Mississippi State University for support of D.L.W. Any opinions, findings, and conclusions or recommendations expressed in this material are those of the authors and do not necessarily reflect the views of the National Science Foundation.

Abbreviations

CA	general abbreviation for human carbonic anhydrase II
ZnCA	Active CA containing a mononuclear Zn^{2+} center
apoCA	CA where the Zn^{2+} ion has been removed
rCA	reconstituted CA by adding Zn^{2+} into apoCA
DPA	dipicolinic acid or pyridine-2,6-dicarboxylic acid
pNPA	p-nitrophenyl acetate
pNP	p-nitrophenol
XAS	X-ray absorption spectroscopy
XANES	X-ray absorption near-edge structure
EXAFS	Extended X-ray absorption fine structure
BVS	bond-valence sum
IPTG	Isopropyl β-D-1-thiogalactopyranoside

Reference

1. Krishnamurthy VM, Kaufman GK, Urbach AR, Gitlin I, Gudiksen KL, Weibel DB, Whitesides GM. Chem. Rev. 2008; 108:946–1051. [PubMed: 18335973]
2. Silverman DN, McKenna R. Acc. Chem. Res. 2007; 40:669–675. [PubMed: 17550224]
3. Linskog S. Pharmacol. Ther. 1997; 74:1–20. [PubMed: 9336012]
4. Christianson DW, Fierke CA. Acc. Chem. Res. 1996; 29:331–339.
5. Silverman DN, Lindskog S. Acc. Chem. Res. 1988; 21:30–36.
6. Smith KS, Jakubzick C, Whittam TS, Ferry JG. Proc. Natl. Acad. Sci. USA. 1999; 96:15184–15189. [PubMed: 10611359]
7. Alber BE, Colangelo CM, Dong J, Stalhandske CMV, Baird TT, Tu C, Fierke CA, Silverman DN, Scott RA, Ferry JG. Biochemistry. 1999; 38:13119–13128. [PubMed: 10529183]
8. Coleman JE. Curr. Opin. Chem. Biol. 1998; 2:222–234. [PubMed: 9667939]
9. Okrasa K, Kazlauskas RJ. Chem. Eur. J. 2006; 12:1587–1596. [PubMed: 16416502]
10. Hunt JA, Ahmed M, Fierke CA. Biochemistry. 1999; 38:9054–9062. [PubMed: 10413479]
11. Hunt JA, Fierke CA. J. Biol. Chem. 1997; 272:20364–20372. [PubMed: 9252341]
12. DiTusa CA, Christensen T, McCall KA, Fierke CA, Toone EJ. Biochemistry. 2001; 40:5338–5344. [PubMed: 11330996]
13. Coleman JE. J. Biol. Chem. 1967; 242:5212–5219. [PubMed: 4965135]
14. Nair SK, Calderone TL, Christianson DW, Fierke CA. J. Biol. Chem. 1991; 266:17320–17325. [PubMed: 1910042]
15. Alexander RS, Kiefer LL, Fierke CA, Christianson DW. Biochemistry. 1993; 32:1510–1518. [PubMed: 8431430]
16. Hunt JB, Rhee MJ, Storm CB. Anal. Biochem. 1977; 79:614–617. [PubMed: 405888]

17. Le V, Buscaglia R, Chaires JB, Lewis EA. Anal. Biochem. 2012 submitted.
18. George, GN. EXAFSPAK. Stanford Synchrotron Radiation Lightsource; Stanford, CA: 2000.
19. Zabinsky SI, Rehr JJ, Ankudinov A, Albers RC, Eller MJ. Phys. Rev. B. 1995; 52:2995–3009.
20. Wang S, Lee MH, Hausinger RP, Clark PA, Wilcox DE, Scott RA. Inorg. Chem. 1994; 33:1589–1593.
21. Riggs-Gelasco PJ, Stemmler TL, Penner-Hahn JE. Coord. Chem. Rev. 1995; 144:245–286.
22. Brown ID, Altermatt D. Acta Cryst. 1985; B41:244–247.
23. Thorp HH. Inorg. Chem. 1992; 31:1585–1588.
24. Kidani Y, Hirose J, Koike H. J. Bio. Chem. 1976; 79:43–51.
25. Pocker Y, Fong CTO. Biochemistry. 1983; 22:813–818. [PubMed: 6838825]
26. Pocker Y, Fong CTO. Biochemistry. 1980; 19:2045–2050. [PubMed: 6769470]
27. Anderegg G. Helv. Chim. Acta. 1960; 43:414–424.
28. Grossoehme NE, Spuches AM, Wilcox DE. J. Biol. Inorg. Chem. 2010; 15:1183–1191. [PubMed: 20725755]
29. Emerson JP, Le VH, Lewis EA. eLS. 2012 in press.
30. Quinn, CF. PhD thesis. Dartmouth College; 2009.
31. Goldberg RN, Kishore N, Lennen RM. J. Phys. Chem. Ref. Data. 2002; 31:231–370.
32. Grossoehme NE, Akilesh S, Guerinot ML, Wilcox DE. Inorg. Chem. 2006; 45:8500–8508. [PubMed: 17029360]
33. King RW, Roberts GK. Biochemistry. 1971; 10:558–565. [PubMed: 4993463]
34. Jacquamet L, Aberdam D, Adrait A, Hazemann JL, Latour JM, Michaud-Soret I. Biochemistry. 1998; 37:2564–2571. [PubMed: 9485406]
35. Giachini L, Veronesi G, Francia F, Venturoli G, Boscherini F. J. Synchrotron Rad. 2010; 17:41–52.
36. Cox EH, McLendon GL, Morel FMMM, Lane TW, Prince RC, Pickering IJ, George GN. Biochemistry. 2000; 39:12128–12130. [PubMed: 11015190]
37. Yachandra V, Powers L, Spiro TG. J. Am. Chem. Soc. 1983; 105:6596–6604.
38. HÅkansson K, Lindahl M, Svensson G, Albertsson J. Acta Chem. Scand. 1993; 47:449–455.
39. NIST Standard Reference Database 46. version 7.0. National Institute of Standards and Technology; Gaithersburg, MD: 2003.
40. Rich AM, Bombarda E, Schenk AD, Lee PE, Cox EH, Spuches AH, Hudson LD, Kieffer B, Wilcox DE. J. Am. Chem. Soc. 2012; 134:10405–10418. [PubMed: 22591173]
41. Avvaru BS, Busby SA, Chalmers MJ, Griffin PR, Venkatakrishnan B, McKenna MA, Silverman DN, Mckenna R. Biochemistry. 2009; 48:7365–7372. [PubMed: 19583303]

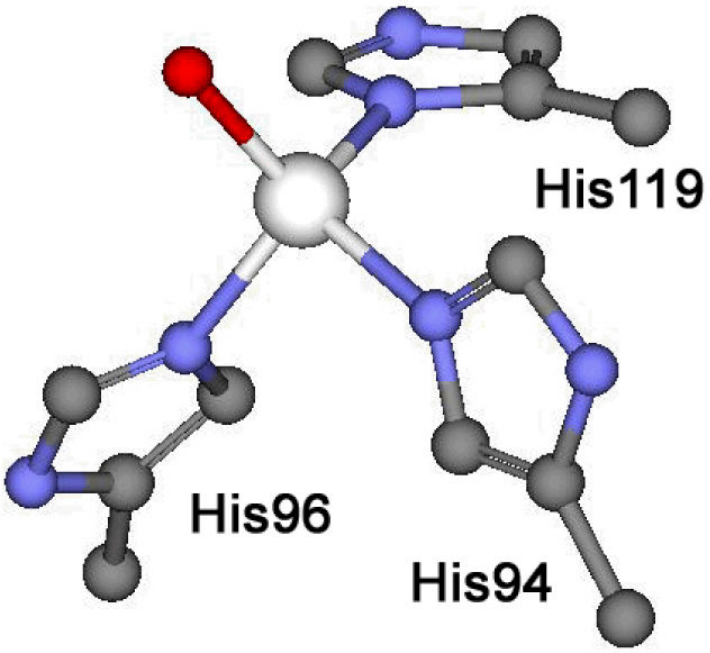

Figure 1.

Zinc coordination site structure of human Carbonic anhydrase II. Image generated using Accelrys Discovery Studio Visualizer 2.5 from coordinates associate with 2CBA.pdb.

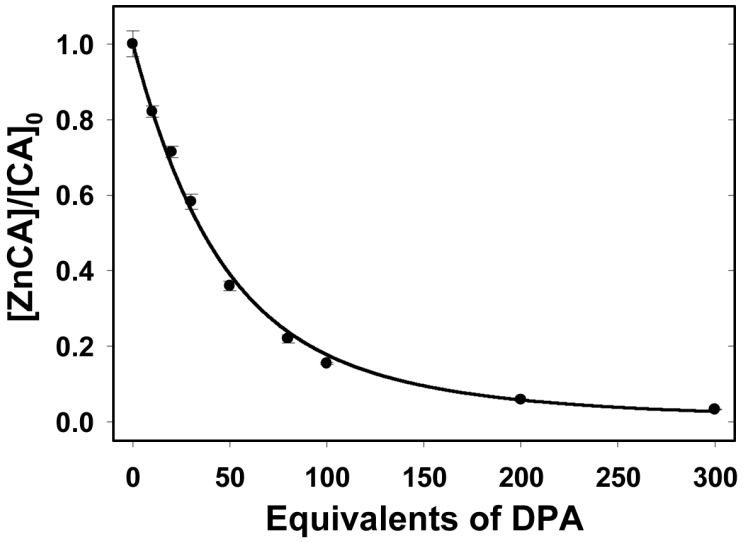

Figure 2.

Inactivation of ZnCA after incubation with the Zn^{2+} chelator DPA. The fraction of active enzyme in each trial is calculated using the rate of ZnCA catalyzed hydrolysis of *p*-nitrophenyl acetate (p-NPA) in various concentrations of DPA. The catalytic rate of each trial then was normalized with the uninhibited hydrolysis (i.e. the same as $[ZnCA]_0$ with 0 equivalents of DPA). All values reported are averages of at minimum 3 trials and error values are derived from standard deviation. Reactivity was monitored by measuring formation of p-nitrophenol (ε_{404} = 17,300 M^{-1} 404 cm^{-1}). All trials done in the presence of dipicolinic acid (DPA) were completed after a 24 hour incubation period at room temperature to insure all solutions achieved equilibrium. Regression line is derived from equation 9.

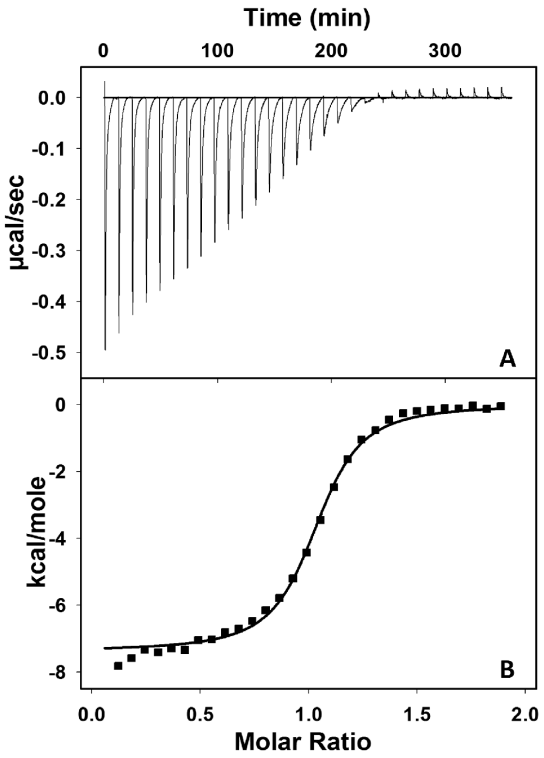

Figure 3.

Isothermal titration calorimetry data of zinc binding to apoCA. (A) Raw data from the titration of a 1.5 mL cell containing 60 µM apoCA was titrated with 30 × 3 µL of 1.73 mM $Zn(NO_3)_2$ in 100 mM ACES at pH 7.4. Injection interval is 12 min. (B) integrated isotherm and the best associated fit for a one-site binding model. The average thermodynamic parameters associated with Zn^{2+} binding to apoCA are reported in Table 1.

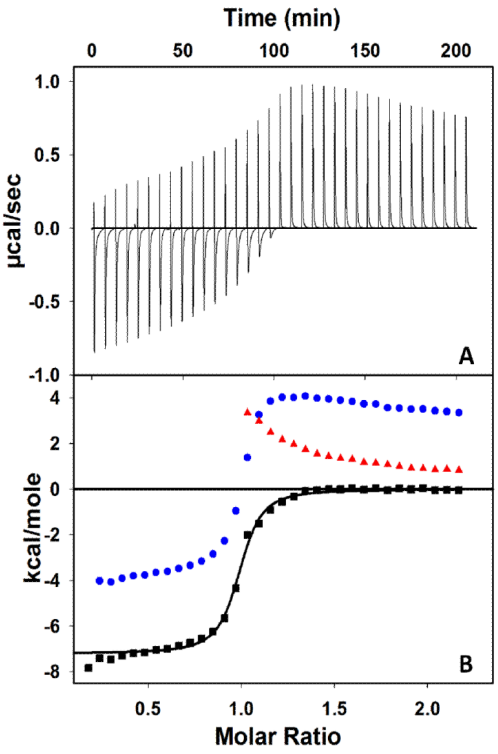

Figure 4.

Isothermal titration calorimetry data of zinc binding to apoCA. (A) Raw data from the titration of a 1.5 mL cell containing 80 µM apoCA was titrated with 35 × 3 µL of 2.26 mM $Zn(NO_3)_2$ in 100 mM PIPES at pH 7.4. (B) Blue: integrated raw data. Red: Integrated Zn^{2+}-buffer background titration. Black: Corrected Zn^{2+} binding isotherm and the best associated fit for a one-site binding model. The average thermodynamic parameters associated with Zn^{2+} binding to apoCA are reported in Table 1.

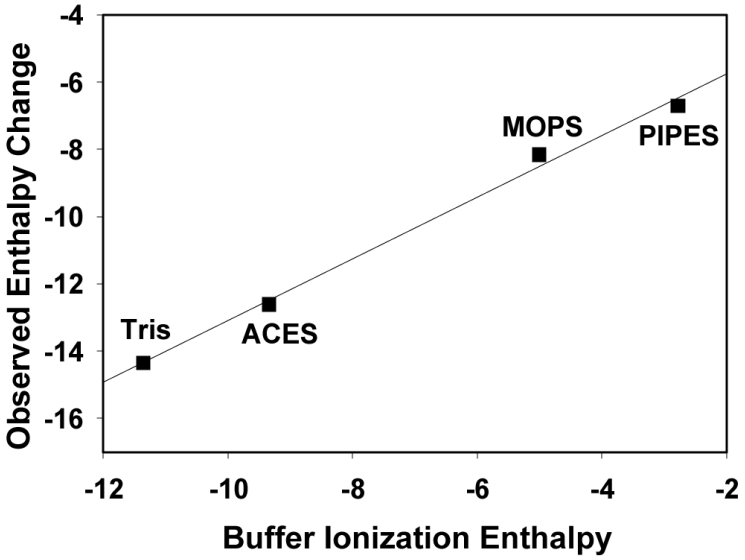

Figure 5.

Plot of the addition of observed enthalpy from ITC and metal-buffer interaction enthalpy ($\Delta H_{ITC} + \Delta H_{Zn\text{-}Buffer}$) versus buffer ionization enthalpies ($\Delta H_{H\text{-}Buffer}$) in various buffers at pH 7.4. Values for ΔH_{ITC}, $\Delta H_{Zn\text{-}Buffer}$ and $\Delta H_{H\text{-}Buffer}$ in various buffers are listed in Table 1 and Table S1. Linear regression values: $y = 0.92 \times - 3.92$. $R^2 = 0.99$.

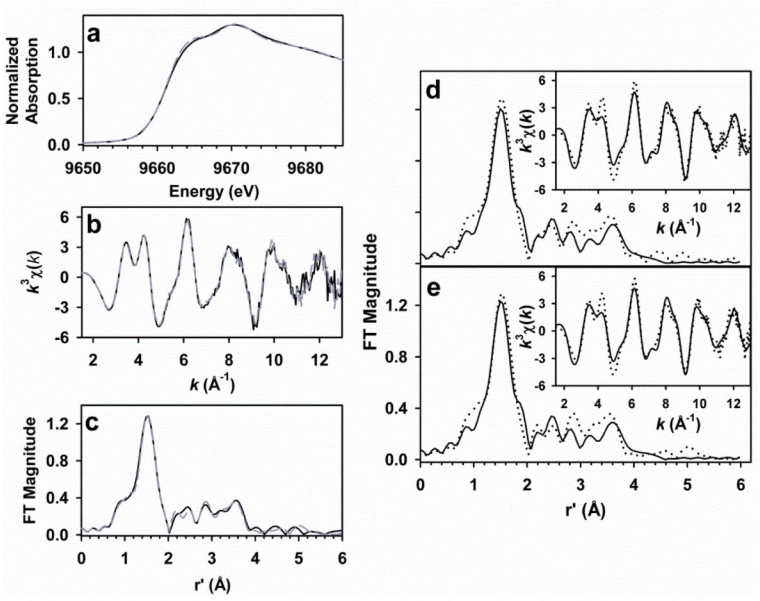

Figure 6.

(left) Comparisons of the XAS data obtained for as-isolated (solid black line) and reconstituted (dashed grey line) ZnCA. The XANES spectra (**a**), $k^3\chi(k)$ EXAFS spectra (**b**), and the Fourier transforms (**c**, k = 1.5 – 13.0 Å^{-1}) are essentially superimposable. Fourier transforms of the unfiltered $k^3\chi(k)$ EXAFS data (insets) of as-isolated CA (**d**) and reconstituted CA (**e**). Experimental data are represented by dotted lines, while best fits (given in bold in Table 2) are shown as solid black lines.

Table 1

Best fit values for Zn^{2+} binding to apoCA from ITC experiments

Buffer	n_{ITC}	K_{ITC}	ΔH_{ITC} (kcal/mol)	ΔG_{ITC} (kcal/mol)	$-T\Delta S_{ITC}$ (kcal/mol)
PIPES	0.97	3.3 (±0.3)×10^6	−7.2 ± 0.1	−8.9 ± 0.1	−1.7 ± 0.1
MOPS	1.03	2.2 (±0.3)×10^6	−8.1 ± 0.1	−8.6 ± 0.1	−0.6 ± 0.1
ACES	1.02	1.1 (±0.1)×10^6	−7.4 ± 0.1	−8.2 ± 0.1	−0.8 ± 0.1
Tris	1.05	7.3 (±0.6)×10^6	−12.3 ± 0.3	−9.4 ± 0.1	3.0 ± 0.3

Table 2

Thermodynamic cycle for Zn^{2+} Binding to apoCA in 100 mM PIPES, pH = 7.4

eq	reaction	coeff	ΔH° (kcal/mol)	ΔG° (kcal/mol)
	$Zn(PIPES)^{2+}$ + $(H^+)_{0.9}$-CA → $ZnCA^{2+}$ + 0.9 H^+PIPES + 0.1 PIPES		−7.2[a]	−8.9[a]
1	$Zn(PIPES)^{2+}$ → Zn^{2+} + PIPES	1	−0.46[b]	4.18[b]
2	H^+-CA → H^+ + CA[c]	0.9	13.50[d]	9.27[e]
3	PIPES + H^+ → H^+PIPES	0.9	−2.78[b]	−9.45[b]
4	Zn^{2+} + CA → $ZnCA^{2+}$	1	−16.4	−12.9

[a] From Table 1.

[b] From Table S1.

[c] The reaction actually written as: $(His)_3Zn\text{-}H_2O \rightarrow (His)_3Zn\text{-}OH^- + H^+$, explanation see text.

[d] ref 39.

[e] pK_a of zinc bound water is 6.8, ref 12. ΔG° = −RTln(K_a)

Table 3

Summary of pH- and buffer- independent thermodynamic values for Zn^{2+} binding to apoCA

Buffer	*K*	ΔH° (kcal/mol)	ΔG° (kcal/mol)	−TΔS° (kcal/mol)
PIPES	2.9 (±0.3)×10^9	−16.4 ± 0.1	−12.9 ± 0.1	3.5 ± 0.1
MOPS	1.7 (±0.2)×10^9	−15.8 ± 0.1	−12.6 ± 0.1	3.2 ± 0.1
ACES	1.9 (±0.1)×10^9	−16.4 ± 0.1	−12.6 ± 0.1	3.7 ± 0.1
Average	2.2 × 10^9	−16.2	−12.7	3.5

Table 4

Representative EXAFS fit progressions for as-isolated and reconstituted ZnCA.[a]

		Zn-N/O			Zn•••C(His)					
Sample	**fit**	**n**	**r**	**σ 2**	**n**	**r**	**σ 2**	**F**	**F-factor**	**ΔE0**
	1	4	1.98	3.4				310	0.492	−5.73
	2	4	1.98	3.3	6C	2.99	6.5	224	0.418	−6.34
As-isolated						**2.99**	**6.5**			
	3	**4**	**1.97**	**3.4**	**3His**	**4.19**	**5.7**	**127**	**0.314**	**−6.56**
						4.21	**5.7**			
	4	4	1.98	3.2				284	0.478	−5.70
	5	4	1.98	3.1	6C	2.99	6.8	206	0.406	−6.21
Reconstituted						**2.99**	**7.0**			
	6	**4**	**1.98**	**3.2**	**3His**	**4.19**	**6.0**	**115**	**0.303**	**−6.46**
						4.21	**6.0**			

[a] r is in units of Å; σ^2 is in units of 10^{-3} $Å^2$; ΔE_0 is in units of eV. All fits are to unfiltered EXAFS data, with Fourier transform ranges of k = 1.5 – 13.0 $Å^{-1}$ (resolution = 0.14 Å) for both samples. In fits 3 and 6, the His imidazoles were treated as a rigid body, and included single scattering paths for Zn^{2+}–Cα and both three and four body paths involving Zn^{2+}–N–Cβ/Nβ (Cβ and Nβ are the more distant atoms of the imidazole).